Photochemical Behavior of Antibiotics Impacted by Complexation Effects of Concomitant Metals: A Case for Ciprofloxacin and Cu(II)†

Xiaoxuan Wei,[a] Jingwen Chen,*[a] Qing Xie,[a] Siyu Zhang,[ab] Yingjie Li,[a] Yifei Zhang,[a] and Hongbin Xie[a]

[a] Key Laboratory of Industrial Ecology and Environmental Engineering (MOE), School of Environmental Science and Technology, Dalian University of Technology, Dalian 116024, China

[b] Key Laboratory of Pollution Ecology and Environmental Engineering, Institute of Applied Ecology, Chinese Academy of Science, Shenyang 110016, China

(11 Pages, 3 Texts, 11 Figures, 4 Tables)

Text S1 Determining K_f' for complexation of ciprofloxacin with Cu(II)

The fluorescence spectra of ciprofloxacin (CIP) with different concentrations of concomitant Cu(II) are shown in Fig. S1(a). The fluorescence intensity at λ = 430 nm was used to calculate the complex ratio (n) and the conditional stability constant (K_f'):

$$\lg\left[\frac{(F_0 - F)}{F}\right] = n \lg[\mathrm{Cu(II)}] + \lg K_f' \quad \text{(S1)}$$

where F_0 and F are the fluorescence intensities of CIP and the Cu(II)-CIP mixture, respectively. As shown in Fig. S1(b), n = 1.05 and $\lg K_f'$ = 6.09, indicating that Cu(II) and CIP can form 1:1 complex with a conditional stability constant $K'_{f,Cu(CIP)} = 1.23 \times 10^6$ in the pH = 7.5 solutions.

† Electronic Supplementary Information (ESI) available: details of the total ion chromatograms and mass spectra of the identified products, the product yields, and the formation and degradation rate constants.

* Correspondence to: Jingwen Chen, e-mail: jwchen@dlut.edu.cn; Phone: +86-411-8470 6269

[a] Dalian University of Technology

[b] Institute of Applied Ecology, Chinese Academy of Science

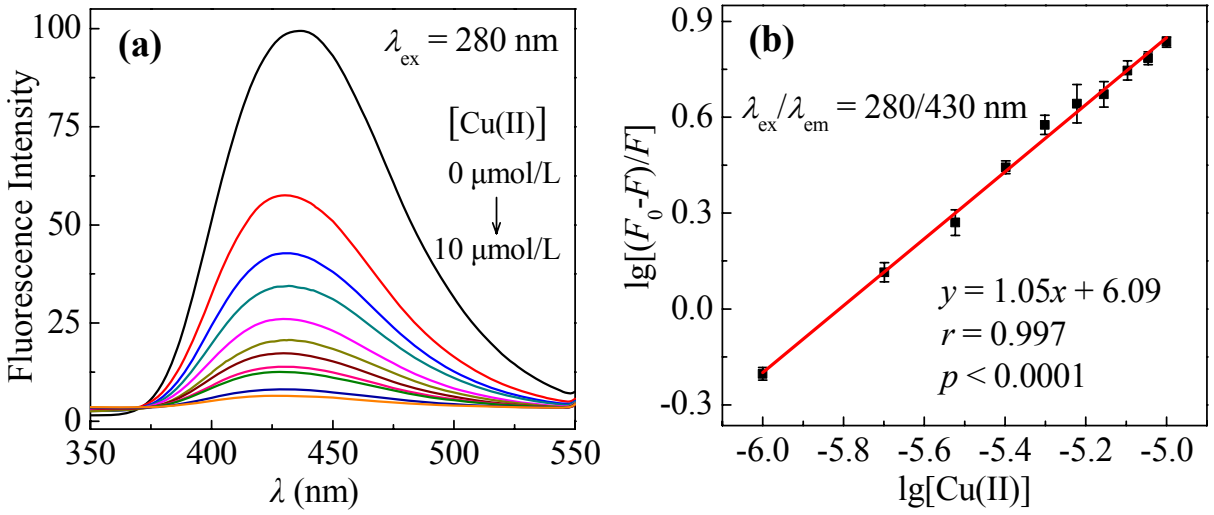

Fig. S1 Effects of Cu(II) on fluorescence intensity of CIP in pH = 7.5 solutions ([CIP] = 0.5 μmol/L, the error bars represent the 95% confidence interval, n = 3)

Text S2 Preparation of Cu(II)-CIP complex

$CuCl_2$ (2.5 mol/L, 20.0 μL) was added to a solution of 1.0 mmol/L CIP (50 mL) with continuous stirring. pH of the mixed solution was adjusted to 7.5. The formed blue crystals of the complex were filtered, washed and dried to constant weight. Subsequently, the solid samples were analyzed by IR, and the results are shown in Fig. S3.

Text S3 DFT calculations of defluorination reactions

The structures of reactants (R), transition states (TS) and products (P) for the C−F bond cleavage of H_2CIP^+ at the excited triplet state (T) and $[Cu(H_2CIP)(H_2O)_4]^{3+}$ at the excited tripquartet state (^{4}T, where the quartet superscript refers to the total spin of the complex, T refers to the local multiplicity of H_2CIP^+) are shown in Fig. S7. Results show that for H_2CIP^+, the distance of C_{12}−F was elongated from 1.35 Å in R to 1.48 Å in the TS, and to 3.86 Å in the P, indicating the rupture of the C−F bond. $[Cu(H_2CIP)(H_2O)_4]^{3+}$ underwent a similar C−F bond cleavage process. The distance of C_{12}−F was elongated from 1.34 Å in the R to 1.93 Å in the TS, and to 3.83 Å in the P. Thus, the Cu(II) complexation has negligible effects on the C−F bond cleavage process of H_2CIP^+.

For the reactions of H_2CIP^+ at the T state and $[Cu(H_2CIP)(H_2O)_4]^{3+}$ at the ^{4}T state with OH^- at its ground state (Fig. S8), two transition states (TS1 and TS2), and one intermediate (IM) were identified, indicating that the OH^- addition reactions are stepwise. The reactions are initiated by the formation of reactant complexes (RCs) between the CIP species and OH^- with different interactions. For H_2CIP^+, intermolecular hydrogen bonds are formed between O in

OH^- and H_{42} (connected with N_{15}) in CIP, whereas for $[Cu(H_2CIP)(H_2O)_4]^{3+}$, intermolecular hydrogen bonds are formed between O in OH^- and H_{40} (connected with C_{20}) in CIP. The subsequent reaction processes are similar for the two species, that is, O in OH^- gradually approaches C_{12} and the distances of C_{12}−O in the IM are reduced to 1.39 Å, falling in the range of a C−O single bond length. In the following step, the distances of C_{12}−F bonds are elongated to about 2.00 Å in TS2. Finally, F^- and hydroxyl products are formed, with the C_{12}−O bond length being < 1.35 Å and the C_{12}−F bond length being > 3.54 Å. Thus, the Cu(II) complexation can alter the OH^- addition reaction channels of H_2CIP^+.

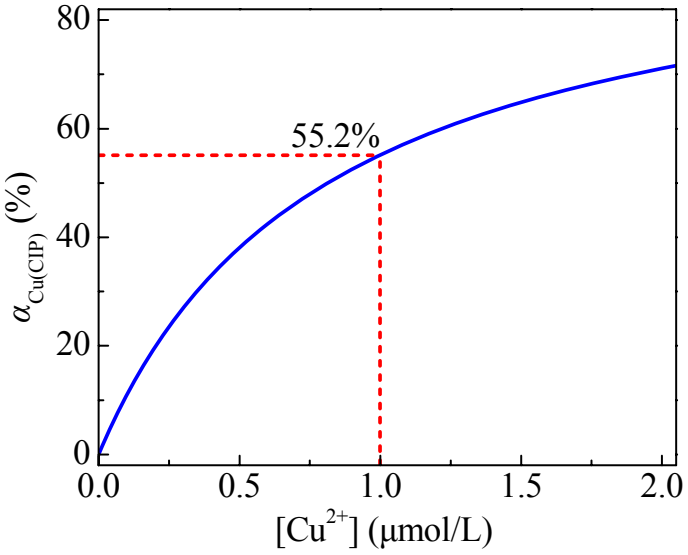

Fig. S2 Effects of equilibrium concentrations of Cu^{2+} on the fraction of Cu(CIP)

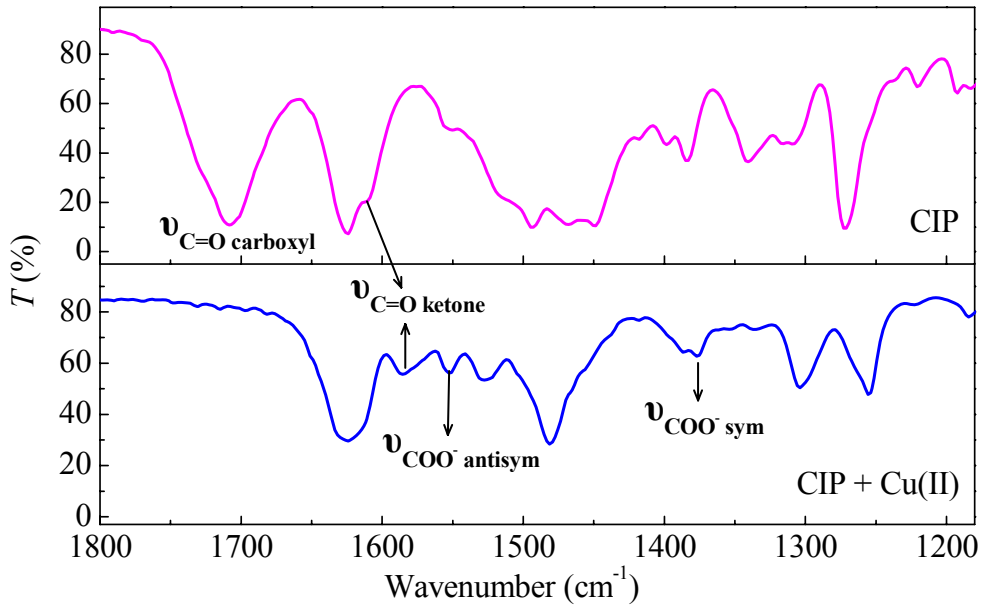

Fig. S3 IR spectra for CIP and mixture of CIP and Cu(II)

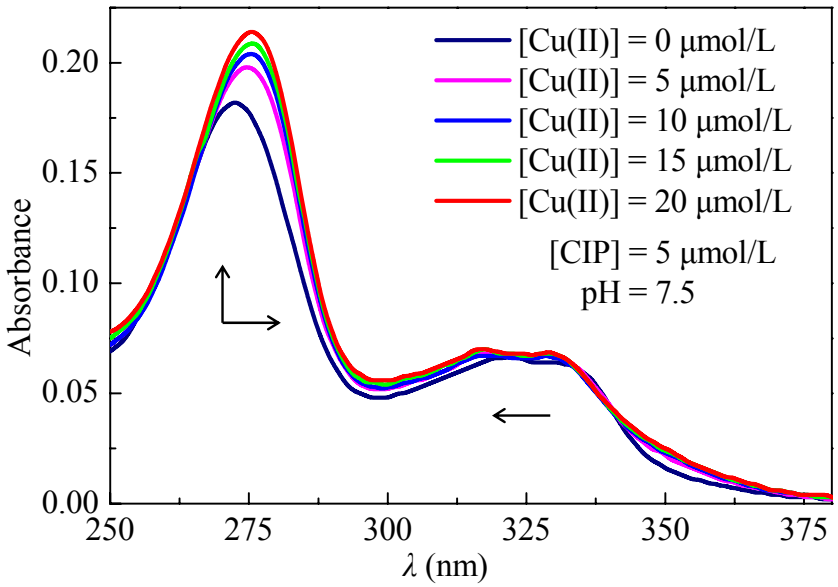

Fig. S4 Variation of UV-vis absorbance spectra of CIP with different [Cu(II)]

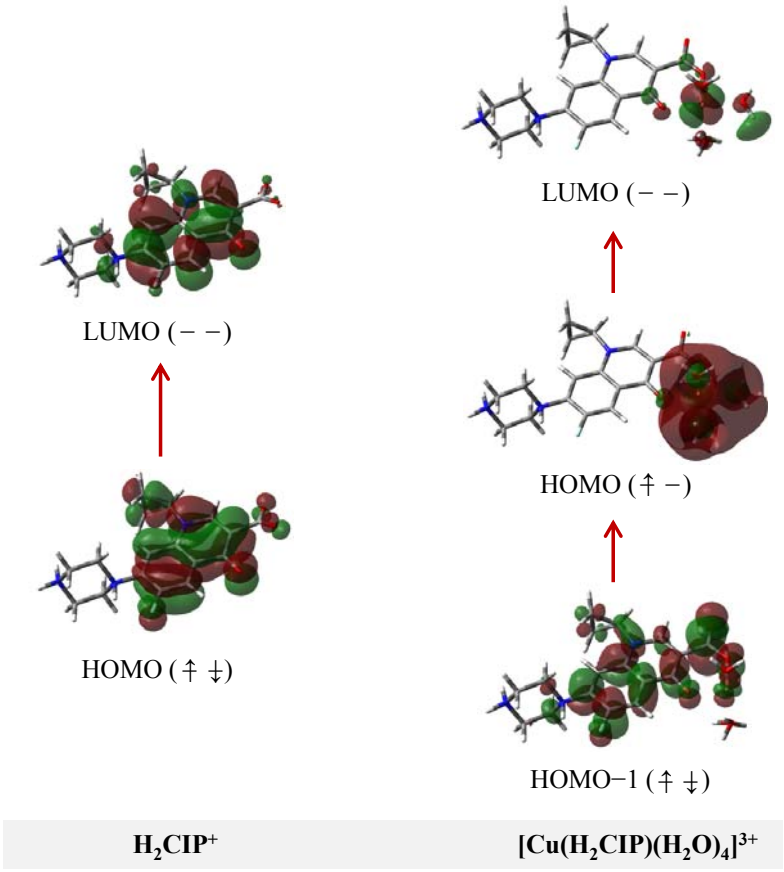

Fig. S5 Molecular orbital compositions and structures for the main absorption of H_2CIP^+ and $[Cu(H_2CIP)(H_2O)_4]^{3+}$ (Piperazine ring to the left, carboxylic group and Cu atom to the right of each molecule. HOMO stands for the highest occupied molecular orbital. HOMO−1 is the second highest occupied molecular orbital. LUMO stands for the lowest unoccupied molecular orbital)

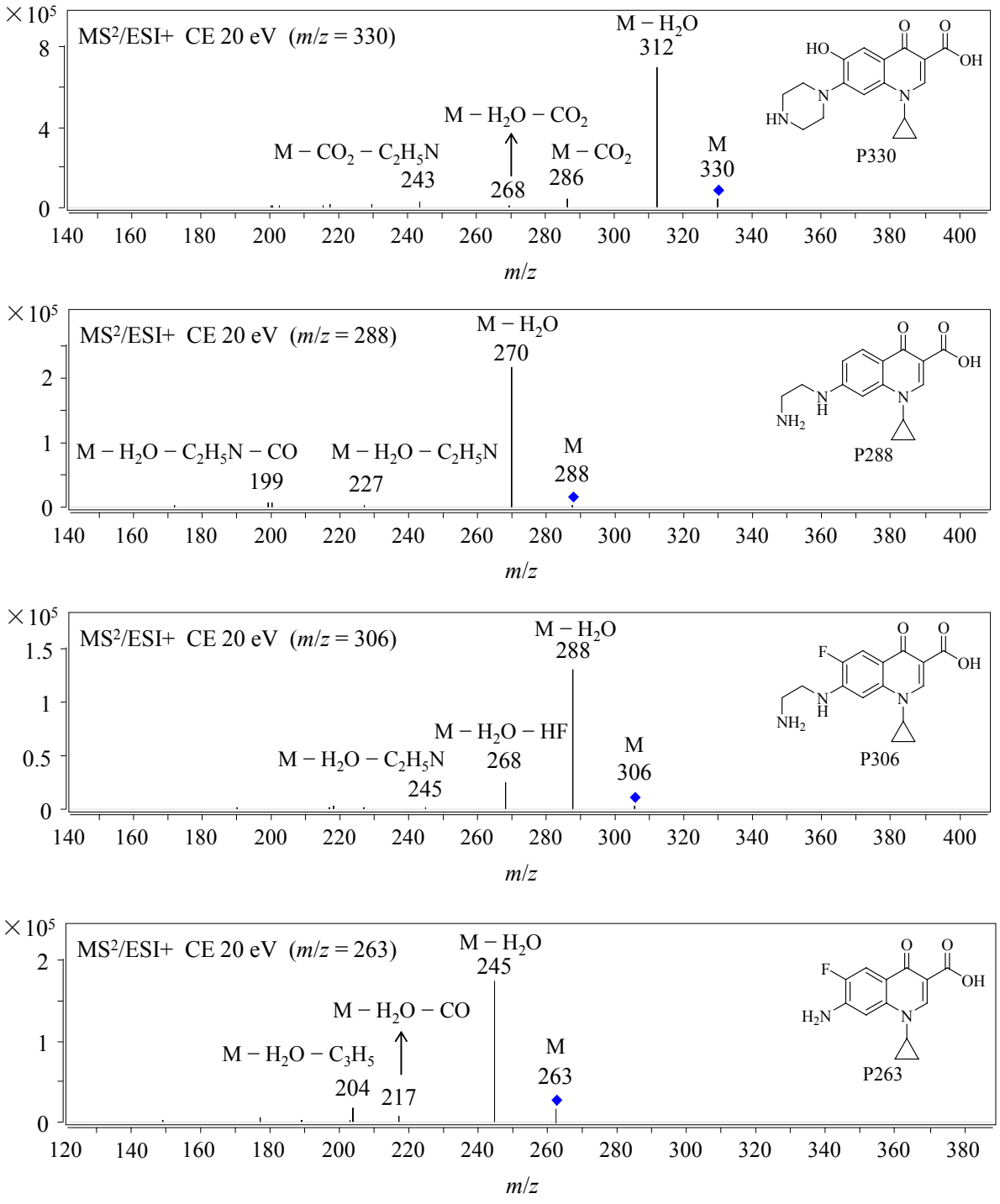

Fig. S6 Mass spectral fragmentation patterns determined by triple quadrupole mass spectrometer for CIP and its photoproducts, where CE stands for collision energy

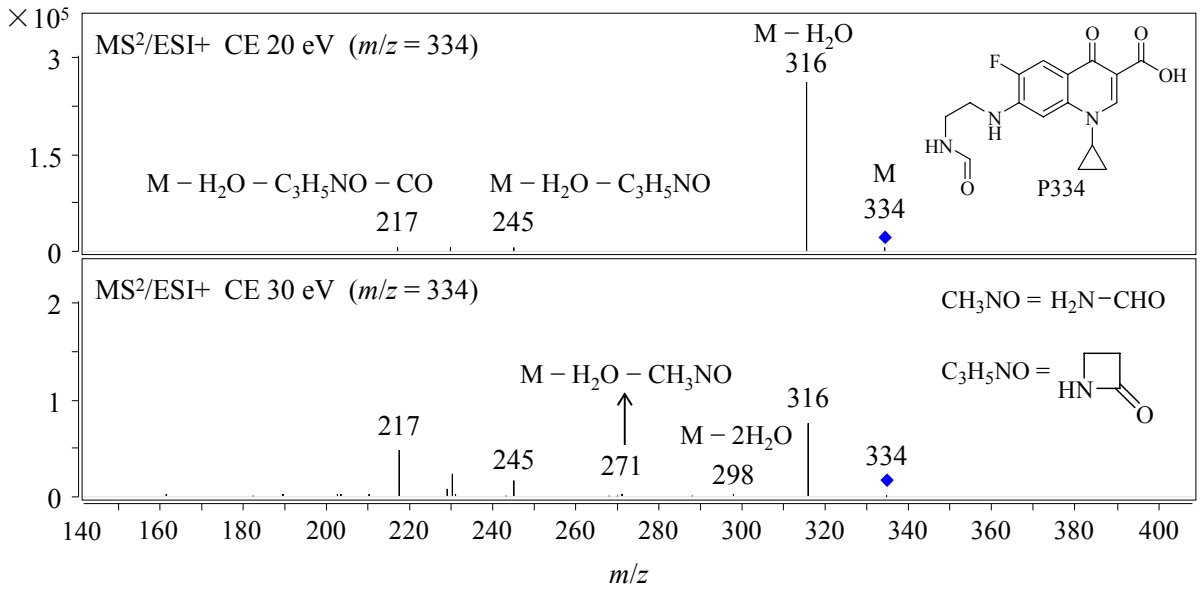

Continued Fig. S6 Mass spectral fragmentation patterns determined by triple quadrupole mass spectrometer for CIP and its photoproducts, where CE stands for collision energy

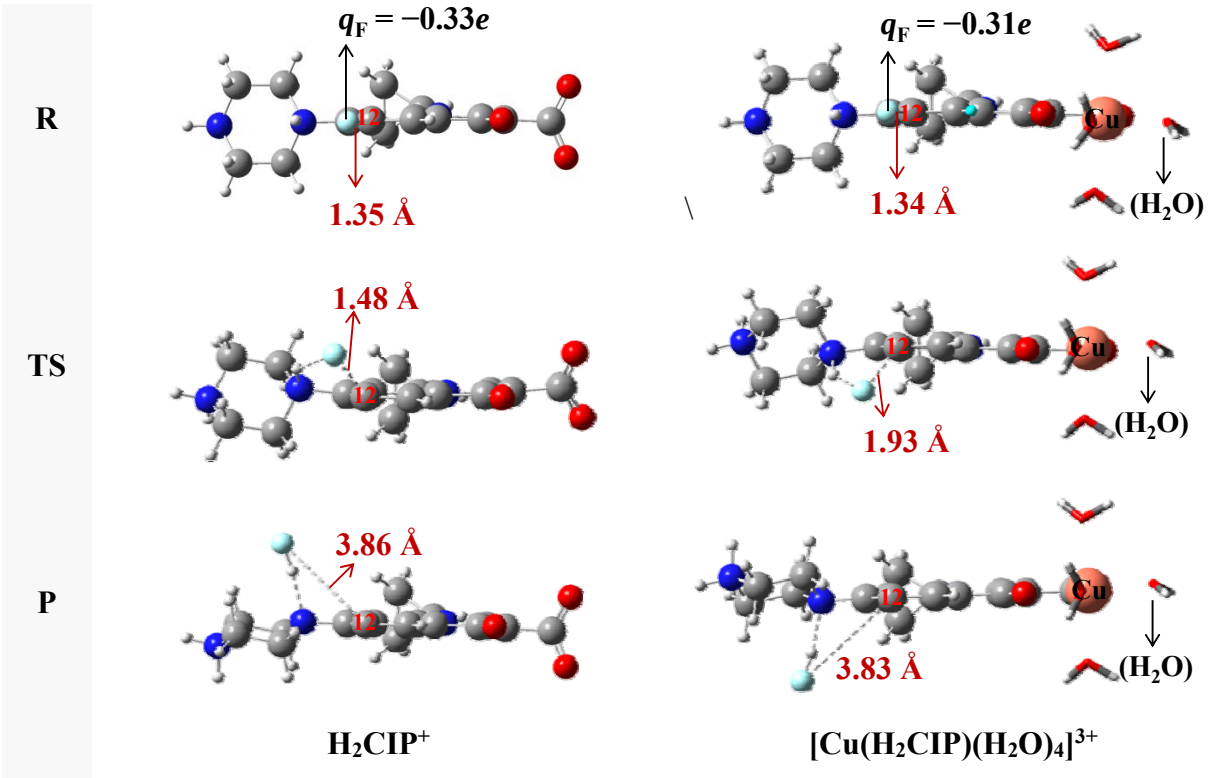

Fig. S7 Optimal structures of the reactants (R), transition states (TS) and products (P) for the C−F bond cleavage of H_2CIP^+ at the T state and $[Cu(H_2CIP)(H_2O)_4]^{3+}$ at the ^4T state (Dark gray: C; Blue: N; Red: O; Light gray: H; Light blue: F; Salmon pink: Cu. q_F stands for the atomic charges on atom F)

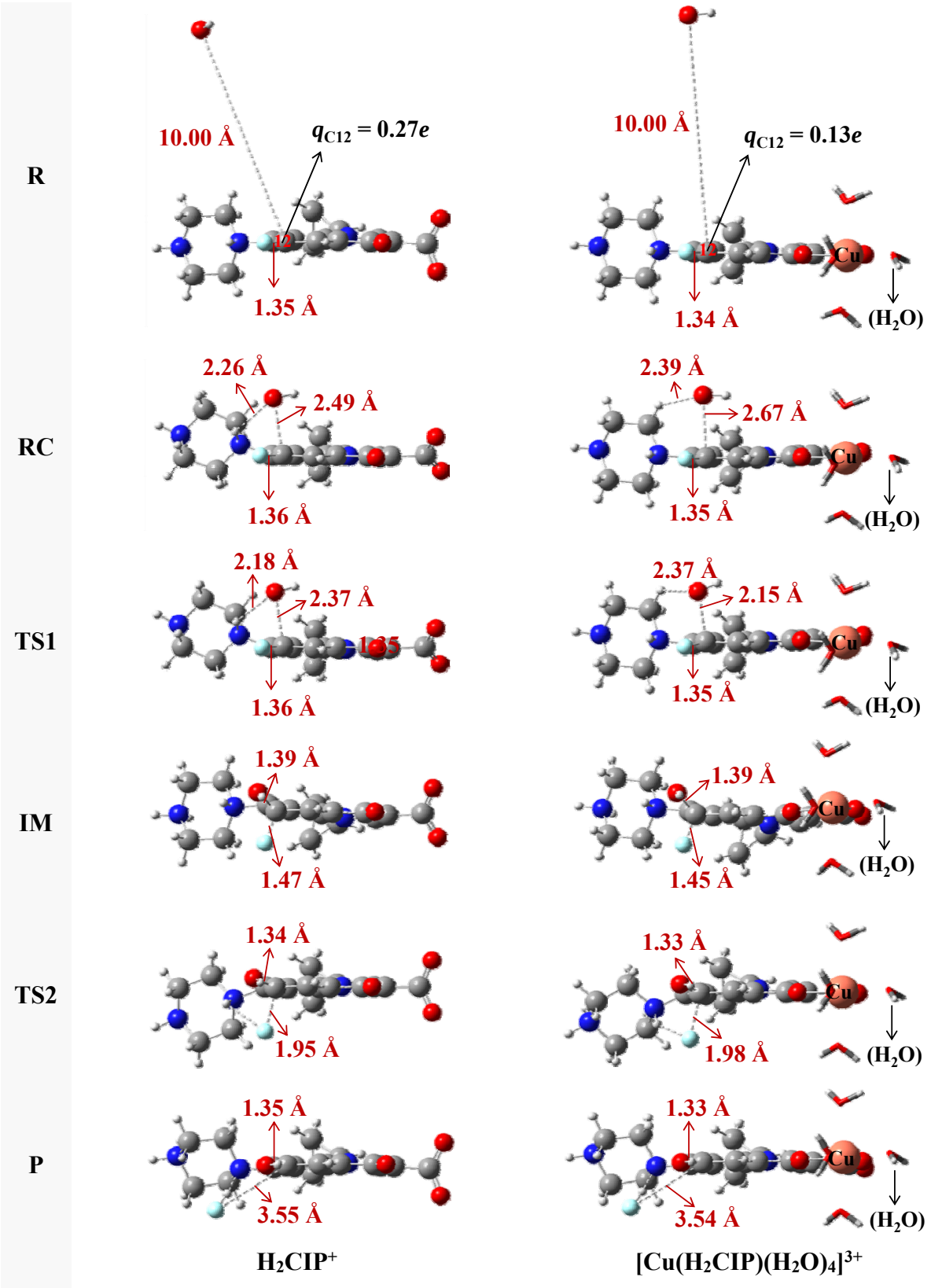

Fig. S8 Optimal structures of the reactants (R), reactant complexes (RC), transition states (TS), intermediates (IM) and products (P) for the reactions of H_2CIP^+ at the T state and $[Cu(H_2CIP)(H_2O)_4]^{3+}$ at the ^4T state with OH^- at its ground state (Dark gray: C; Blue: N; Red: O; Light gray: H; Light blue: F; Salmon pink: Cu. q_{C12} stands for the atomic charges on C_{12})

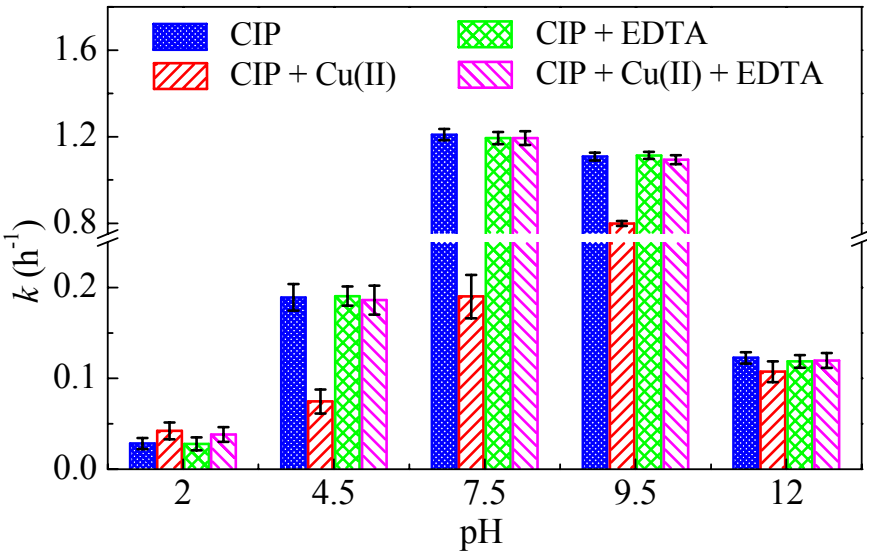

Fig. S9 Effects of pH, Cu(II) and EDTA on the apparent photolytic rate constants (k) of CIP in aerated solutions, where $[CIP]_0$ = 5 μmol/L, [Cu(II)] = 10 μmol/L, [EDTA] = 20 μmol/L and the error bars represent the 95% confidence interval, n = 3

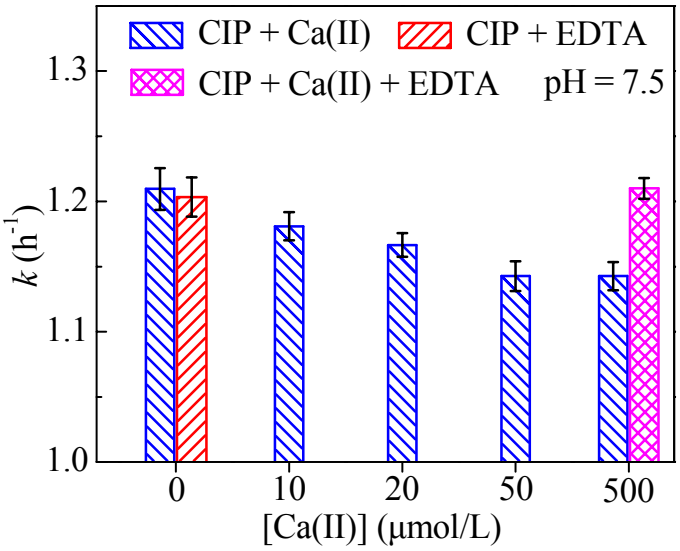

Fig. S10 Effects of Ca(II) and EDTA on the apparent photolytic rate constants (k) of CIP in aerated solutions ($[CIP]_0$ = 5 μmol/L, [EDTA] = 1 mmol/L. The error bars represent the 95% confidence interval, n = 3)

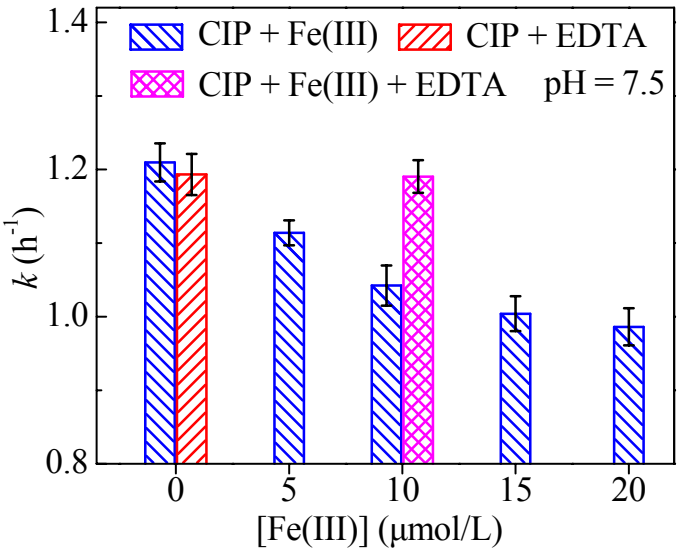

Fig. S11 Effects of Fe(III) and EDTA on the apparent photolytic rate constants (k) of CIP in aerated solutions ($[CIP]_0$ = 5 μmol/L, [EDTA] = 20 μmol/L. The error bars represent the 95% confidence interval, n = 3)

Table S1 Main light absorption wavelength (λ, nm), orbital compositions, and oscillator strengths of H_2CIP^+ and $[Cu(H_2CIP)(H_2O)_4]^{3+}$

λ (nm)	Orbital Components*	Oscillator Strengths
	H_2CIP^+	
322.3	H→L (0.59)	0.118
273.8	H→L+1 (0.66)	0.158
	$[Cu(H_2CIP)(H_2O)_4]^{3+}$	
315.5	H−1→H (0.69); H→L (0.68)	0.244
278.6	H−1→L+1 (0.62); H→L+1 (0.63)	0.106

*The main orbital components of the absorptions are given relative to the highest occupied (H) and lowest unoccupied (L) molecular orbitals and their respective contributions.

Table S2 Accurate mass measurements determined by TOF mass spectrometer for CIP and its photoproducts

Name	Proposed formula $[M + H]^+$	Experimental mass (m/z)	Calculated mass (m/z)	Error (ppm)	DBE*
CIP	$C_{17}H_{19}FN_3O_3$	332.1400	332.1405	1.50	10
P330	$C_{17}H_{20}N_3O_4$	330.1441	330.1448	2.23	10
P288	$C_{15}H_{18}N_3O_3$	288.1335	288.1343	2.67	9
P306	$C_{15}H_{17}FN_3O_3$	306.1243	306.1248	1.79	9
P334	$C_{16}H_{17}FN_3O_4$	334.1197	334.1198	0.18	10
P263	$C_{13}H_{12}FN_2O_3$	263.0825	263.0826	0.56	9

* DBE stands for double bond equivalents.

Table S3 Computed Gibbs free energy changes (ΔG, kcal/mol), enthalpy changes (ΔH, kcal/mol) and activation free energies ($\Delta G^{\ddagger}$, kcal/mol) for the defluorination reactions of H_2CIP^+ and $[Cu(H_2CIP)(H_2O)_4]^{3+}$

	ΔG (kcal/mol)	ΔH (kcal/mol)	$\Delta G^{\ddagger}$ (kcal/mol)
Cleavage of the C−F Bonds			
H_2CIP^+	−4.8	−2.8	27.3
$[Cu(H_2CIP)(H_2O)_4]^{3+}$	−1.4	−0.6	32.8
Defluorination caused by OH^- Addition			
H_2CIP^+	−68.8	−71.9	0.8, 6.0 *
$[Cu(H_2CIP)(H_2O)_4]^{3+}$	−51.0	−52.6	4.5, 10.8 *

* OH^- addition reactions are stepwise. The two $\Delta G^{\ddagger}$ values correspond to the process of OH^- attack and cleavage of C−F bond, respectively. Cleavage of C−F bond is a rate-limiting step.

Table S4 Optimized geometries and Mulliken atomic charges of H_2ClP^+ and $[Cu(H_2ClP)(H_2O)_4]^{3+}$ at ground state (Dark gray: C; Blue: N; Red: O; Light gray: H; Light blue: F; Salmon pink: Cu)

Atom	Atomic Charges	
	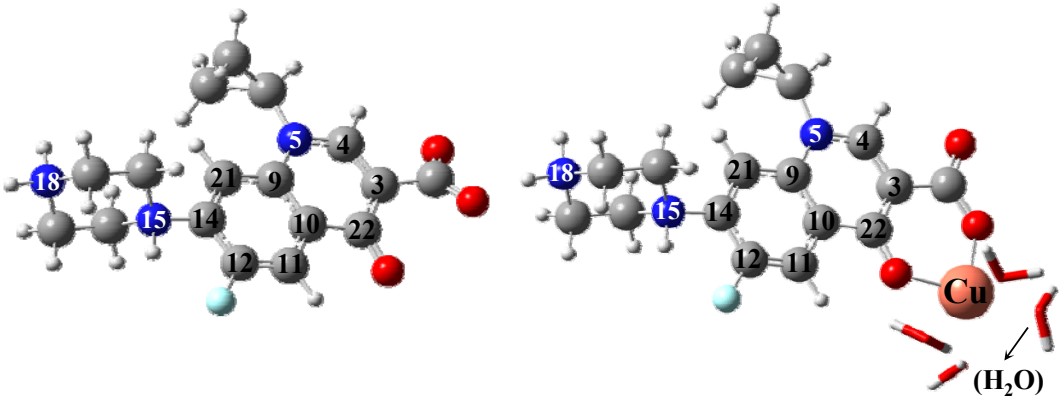	
	H_2ClP^+	$[Cu(H_2ClP)(H_2O)_4]^{3+}$
C_3	−0.24*e*	0.43*e*
C_4	−0.33*e*	−0.31*e*
N_5	0.06*e*	0.12*e*
C_9	−0.34*e*	0.20*e*
C_{10}	1.06*e*	0.30*e*
C_{11}	−0.04*e*	−0.32*e*
C_{12}	0.07*e*	0.08*e*
C_{14}	−0.10*e*	0.08*e*
N_{15}	**−0.63*e***	**−0.68*e***
N_{18}	**−0.61*e***	**−0.59*e***
C_{21}	−0.50*e*	−0.25*e*
C_{22}	−0.02*e*	−0.40*e*